ADVANCED FUNCTIONAL MATERIALS
www.afm-journal.de

In Situ Fabrication of Three-Dimensional Graphene Films on Gold Substrates with Controllable Pore Structures for High-Performance Electrochemical Sensing

Lei Shi, Zhenyu Chu, Yu Liu, Wanqin Jin, and Nanping Xu*

In this work, novel three-dimensional graphene films (3D GFs) with controllable pore structures are directly fabricated on gold substrates through the hydrothermal reduction. An interfacial technique of the self-assembled monolayer is successfully introduced to address the binding issue between the graphene film and substrate. Adscititious silica spheres, serving as new connection centers, effectively regulate the dimensions of framework in graphene films, and secondary pore structures are produced once removing the spheres. Based on hierarchically porous 3D GFs with large surface area, excellent binding strength, high conductivity, and distinct interfacial micro-environments, selected examples of electrochemical aptasensors are constructed for the assay of adenosine triphosphate (ATP) and thrombin (Tob) respectively. Sensitive ATP and Tob aptasensors, with high selectivity, excellent stability, and promising potential in real serum sample analysis, are established on 3D GFs with different structures. The results demonstrate that the surface area, as well as interfacial micro-environments, plays a critical role in the molecular recognition. The developed reliable and scalable protocol is envisaged to become a general path for in situ fabrication of more graphene films and the as-synthesized 3D GFs would open up a wide horizon for potential applications in electronic and energy-related systems.

1. Introduction

Graphene, a one-atom-thick planar sheet densely packed with sp^2-bonded carbon atoms, has attracted considerable interest due to its excellent electrical conductivity, high flexibility and mechanical stability, large theoretical specific surface area and unique transport properties.[1,2] Unfortunately, the unavoidable restacking and agglomeration of graphene sheets caused by the van der Waals forces diminishes their accessible surface area, breaks the continuous pathway for electron transport and suppresses the intrinsically mechanical strength of individual graphene sheet.[3,4] Therefore, constructing novel and promising three-dimensional (3D) graphene structures is highly desired for the realization of perfect sheet-to-sheet connectivity of graphene flakes, which would enable important advances in the catalysis, electric capacitors and sensors.[5–10]

Many efforts have recently been dedicated in the construction of 3D graphene structures, which are mainly based on the techniques of the freeze-drying,[11,12] hydrothermal reduction (HR),[13–15] electrochemical reduction,[16–18] and chemical vapor deposition.[19,20] Among these approaches, the HR is considered as one of the most attractive techniques, because of its simplicity, low cost, and especially the green reduction without generating any contamination, due to the simultaneous process of self-assembly and reduction of graphene oxide (GO) sheets. However, two potential problems are accompanied with the HR technique, which would limit the extensive applications of the obtained 3D graphene. One is concerned on that the pore dimensions in the framework of the proposed 3D graphene were usually around several micrometers and few hierarchical pore structures were observed, which significantly restricted their surface area and impaired the availability of the surface. Another involved is that the HR approach is now confined in the preparation of porous graphene monolith, while the in situ fabrication of graphene films on the supporting substrates is stimulated by the enormous demand in the applications of micro/nano devices, smart membranes and electrochemical sensors.[21–24] Therefore, it has remained a great challenge to fabricate novel desired 3D graphene films using the HR technique.

Electrochemical aptasensors have found many significant applications on account of their distinctive properties of high affinity and specificity toward extensive targets, for example, small molecules, biological proteins and cells.[25–27] The development of promising electrode materials with novel 3D structures is considered as a critical strategy to construct an excellent electrochemical biosensor.[28–32] The huge surface area of 3D structures would improve immobilization sites for the biological molecules, provide more interfacial reaction positions and make the molecules easily accessible to electrode surface,

L. Shi, Dr. Z. Y. Chu, Y. Liu, Prof. W. Q. Jin, Prof. N. P. Xu
State Key Laboratory of Materials-Oriented Chemical Engineering
College of Chemistry and Chemical Engineering
Nanjing University of Technology
Nanjing 210009, P. R. China
E-mail: wqjin@njtech.edu.cn

DOI: 10.1002/adfm.201402095

which enhanced the signal acquisition and finally contributed to an increased performance. However, few reports have been focused on the 3D graphene based electrochemical aptasensors.

In this work, for the first time, in situ fabrication of the 3D graphene films (3D GFs) on gold substrates with controllable pore structures was realized by the HR technique. The gold substrate modified with a self-assembled monolayer (SAM) of 4-aminothiophenol was served for the growth of porous graphene films. Silica spheres with different diameters, acting as new connection centers during the self-assembly process of GO sheets, were introduced to regulate the dimensions of framework in the 3D GFs. Meanwhile, secondary pore structures were produced once these spheres were removed, resulting in a hierarchical pore structures. The advancement of the proposed 3D GFs enhanced their applicability in potential applications, and as examples, novel electrochemical aptasensors were constructed based on the 3D GFs, which realized the excellent performance in the assay of ATP and Tob respectively.

2. Results and Discussions

2.1. In Situ Fabrication of the 3D GFs on Gold Substrates

Self-assembled monolayers (SAMs) were extensively applied in the interface chemistry and considered as an effective approach to address the interfacial binding issues.[33–35] Here, a SAM of 4-aminothiophenol was introduced for the growth of the porous graphene films on the gold substrate. As shown in **Figure 1**A, the SAM was formed on the gold surface through the Au-S bond, while the -NH_2 groups at another terminal of SAM would interact with the -COOH groups in GO. The modification time of the gold substrate with 4-aminothiophenol was optimized because the redundant 4-aminothiophenol anchored onto the substrate would increase the transfer resistance of electron. Here, the modification time of 1 h was introduced, in which a subtle decrease in current compared with that of bare gold substrate was observed (shown in Figure S1, Supporting

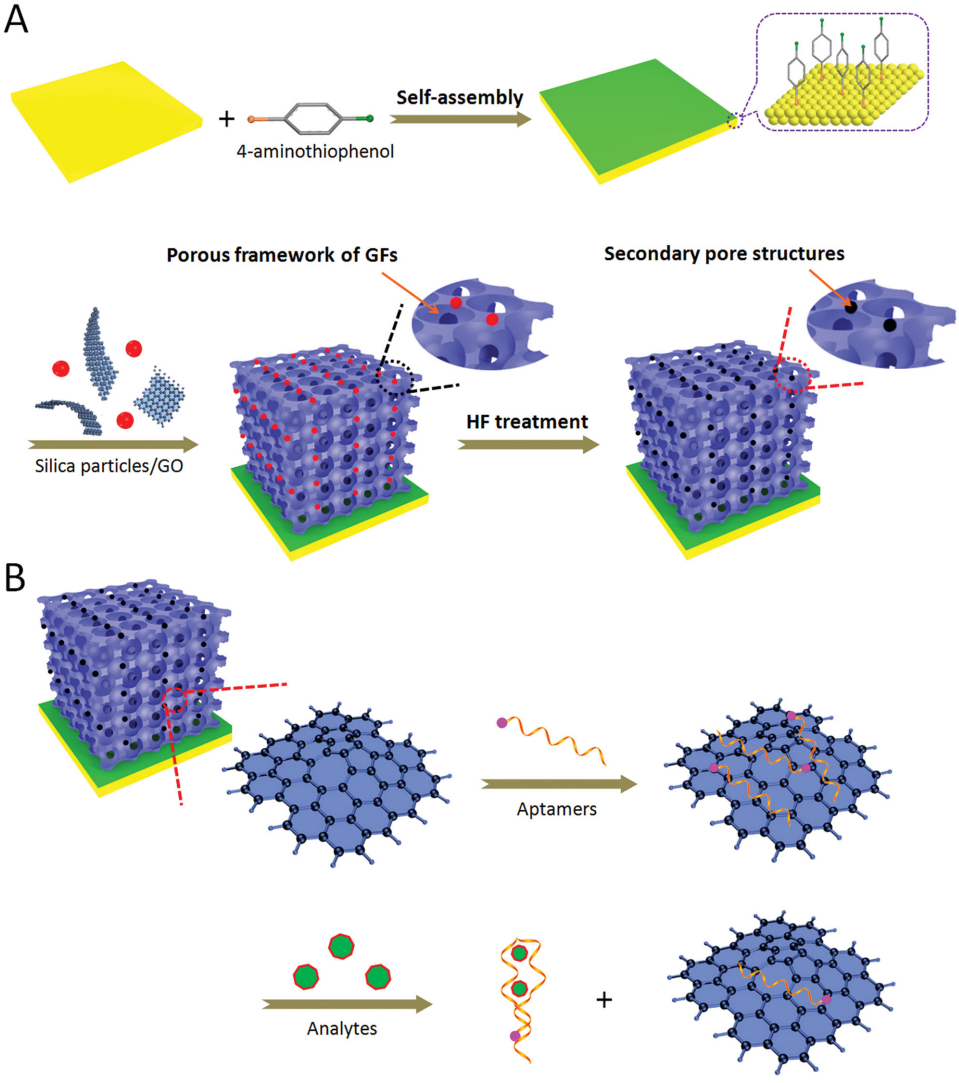

Figure 1. A) Schematic illustration of the fabrication process for 3D GFs. B) Schematic illustration of the 3D GFs based electrochemical aptasensors for the assay of ATP and Tob.

Information). Besides, as the partial overlapping of flexible graphene sheets resulting in the formation of physical cross-linking sites in the framework of porous graphene,[15] the pore dimensions of the framework were dependent on the formed cross-linking sites. Therefore, it would be feasible to adjust the pore sizes through introducing more cross-linking sites. Silica spheres, serving as new connection centers, were adopted in this work. When graphene sheets enwrapped the homogeneously dispersed silica spheres, additional cross-linking sites were created, which effectively reduced the pore dimensions in the framework. Furthermore, secondary pore structures were produced once the spheres embedded in the graphene films were removed. Finally, a hierarchically porous graphene film with significantly enhanced surface area was obtained.

2.2. Characterization of the Fabricated 3D GFs

As shown in **Figure 2**, large-scale and homogeneous 3D GFs were successfully fabricated on the gold substrates, which possessed well-defined and interconnected 3D framework. Particularly, the pore walls consisting of thin layers of stacked graphene sheets were produced, which was essential for realizing the excellent electron transfer in the 3D GFs.[2] In the absence of silica spheres, the obtained pore dimensions in the framework of the GF-1 were up to several micrometers (Figure 2B,C). With the addition of silica spheres of 500 nm, a compact silica-graphene hybrid film was observed (Figure 2D), demonstrating the reliable function of silica spheres as connection centers. While removing the silica spheres, the GF-2 with obviously diminished pore dimensions in the framework was created (Figure 2E,F). Moreover, when silica spheres with a smaller diameter of 250 nm were introduced, the amount of connection centers increased and thus a more compact silica-graphene hybrid film was produced (Figure 2G). In this case, as more cross-linking sites were formed, the pore dimensions in the framework of the GF-3 were further decreased (Figure 2H,I). The results exhibited that the present silica spheres could effectively adjust the pore dimensions of the 3D GFs. Furthermore, because the wettability of the porous structures plays a critical role in their interfacial behaviors,[36,37] the contact angle measurements were implemented in this work. As shown in insets of Figure 2C,F,I, with the decrease of the pore dimensions in the framework, obvious increments in the contact angles ranging from 98.2°, 106.1° to 116.2° were observed. It may be due to that the porous surface with smaller pore dimensions would provide more interspaces for trapping of the air and thus contributed to the larger contact angle.[38] The increased contact angles implied different interfacial micro-environments on the surface of the porous structures. A large contact angle would decrease the accessible surface area and not facilitate the mass transfer at the interfaces, especially in the condition of molecules with large dimensions.

As shown in the cross-section images of the fabricated 3D GFs (**Figure 3**), integrated and uniform GFs were successfully formed on the gold substrates, which were modified with the SAM of 4-aminothiophenol. However, no obvious graphene structures were observed on the substrates in the absence of 4-aminothiophenol SAM (shown in Figure S2, Supporting Information). It was demonstrated that the proposed interface

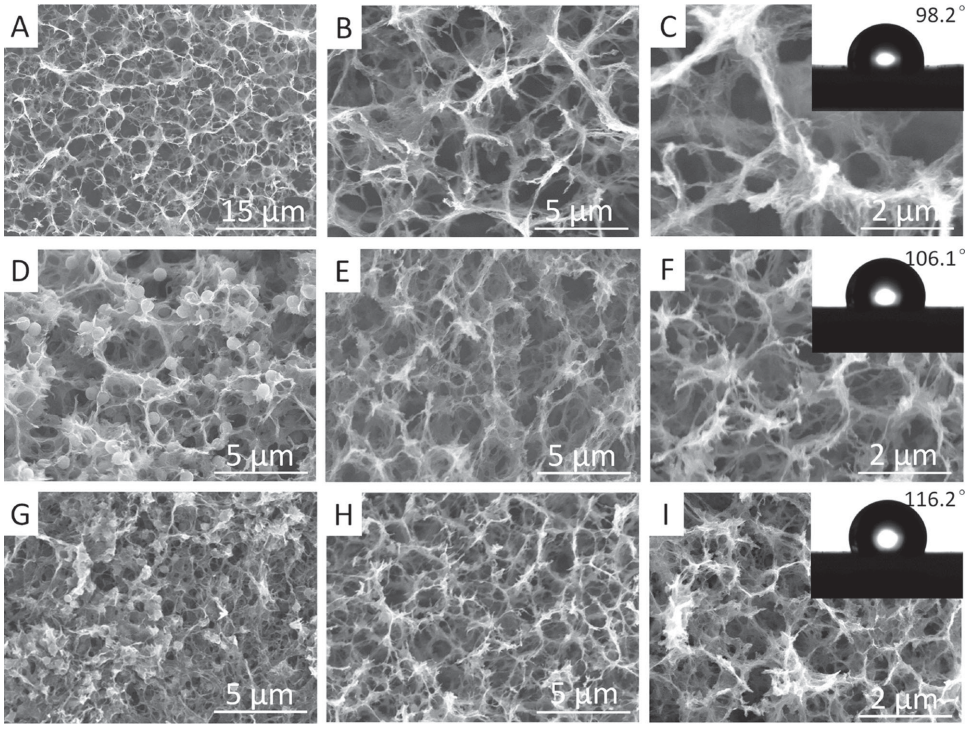

Figure 2. FESEM images of A–C) the fabricated GF-1 with different magnifications, D) the 500 nm silica sphere-graphene hybrid film, E,F) the fabricated GF-2 with different magnifications, G) the 250 nm silica sphere-graphene hybrid film, H,I) the fabricated GF-3 with different magnifications. Insets in (C,F,I) the contact angle measurements of GF-1, GF-2, and GF-3 respectively.

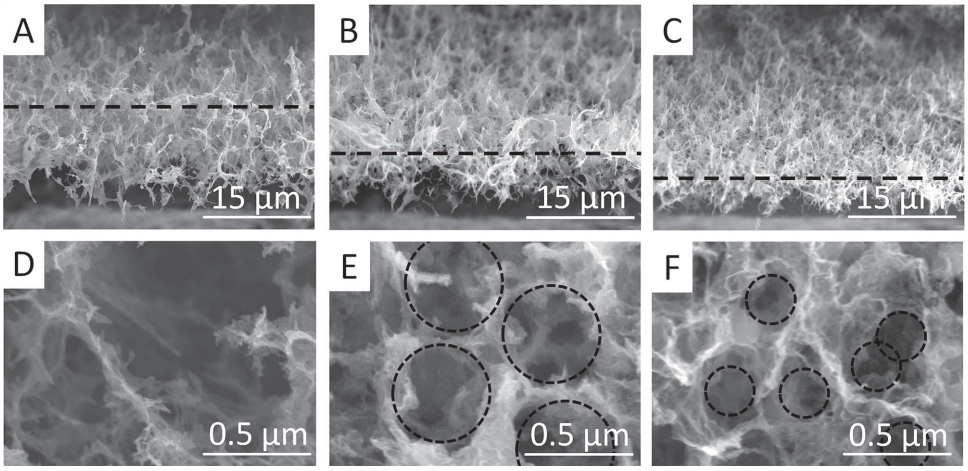

Figure 3. Cross-section images of A) GF-1, B) GF-2, and C) GF-3. D–F) Local magnification images of (A–C).

technique of SAM was critical and feasible to realize the excellent binding strength between the graphene and gold substrate. In addition, it could be seen that a porous film with a thickness of around 15 μm was observed in the GF-1 (Figure 3A), while with the decreased pore dimensions in GF-2 and GF-3, thinner graphene films of ca. 10 μm and 5 μm were obtained respectively (Figure 3B,C). Especially, with a high magnification focused on the porous films, secondary pore structures of around 500 nm and 250 nm were found in the GF-2 and GF-3 respectively (Figure 3E,F), which were produced after removing the silica spheres. In contrast, no similar structures were obtained in the GF-1 (shown in Figure 3D). Definitely, the created secondary pore structures were propitious to further improve the surface area of the porous graphene films.

Moreover, the chemical component and physical properties of obtained 3D GFs were investigated by XPS, XRD, and Raman spectroscopy, and various GFs showed similar properties (not shown here). As shown in **Figure 4**A,B, in the XPS C1s spectra, four peaks centered at 284.8, 286.2, 287.7, and 289.2 eV were assigned to C–C in aromatic rings, C–O (epoxy), carbonyl (C = O), and carboxyl (O–C = O) groups, respectively.[39,40] After the HR treatment (Figure 4B), the peak intensity at 284.8 eV significantly became stronger, together with the fading of peaks at 286.2, 287.7, and 289.2 eV, confirming the removal of most oxygen functional groups and the simultaneous restoration of conjugated network. As a result, the atomic ratio of C1s/O1s increased from 2.5 in the GO to ca. 5.9 in GFs. In addition, in XRD analysis (Figure 4C), the elimination of functional groups led to the decrease of interlayer spacing, from 0.731 nm of GO to 0.355 nm of GFs, while slightly higher than that of natural graphite (0.336 nm). The broad XRD peak of the GFs indicated the poor ordering of graphene sheets along their stacking direction and reflected that the framework of the GFs was composed of few-layer stacked graphene sheets, which was consistent with the results obtained in FESEMs. The results from XPS and XRD also confirmed the presence of residual oxygenated functional groups on GFs. Due to these residual hydrophilic groups, the fabricated GFs possessed the improved wettability and relatively smaller contact angles were observed on the GFs compared with those reported in literatures.[41,42] Furthermore, the Raman spectra of graphite, GO and GFs displayed a D-band at 1340 cm^{-1} and a G-band at 1590 cm^{-1} were shown in Figure 4D. The G-band is attributed to the first-order scattering of the E2g mode, and the D-band is associated with the structural defects related to the partially disordered structures of graphitic domains or created by the attachments of functional groups on the carbon basal plane.[43] The D/G value of GFs was calculated to be 1.03, which was higher than that of GO (0.91), suggesting the formation of new quasi-amorphous sp^2-bonded carbons upon reduction.

Besides, CV, CC and EIS were introduced to investigate the electrochemical behaviors of fabricated 3D GFs. The GFs were firstly electrochemically cycled in a 10 mM $K_3Fe(CN)_6$ containing 3M KCl solution.[44] As shown in **Figure 5**A, obviously increased oxidation peak currents ranging from 19.4 μA (GF-1), 46.1 μA (GF-2) to 63.4 μA (GF-3) were obtained, compared with a low signal of 6.4 μA on the bare gold substrate. It was undoubted that the formed 3D GFs, especially with hierarchically porous structures, significantly enhanced their surface area. However, a decreased peak-to-peak separation of 26.7 μA (from GF-1 to GF-2) to 17.3 μA (from GF-2 to GF-3) was observed, which may be due to the changed interfacial micro-environments caused by the increased contact angles. To investigate the electrochemically active surface area of proposed 3D GFs, the CC curves were implemented.[45] As shown in Figure S3, with the enhanced surface area from bare gold substrate to GFs, the CC curves started at higher charge values due to the increased electric double layer capacitance of the GFs modified electrode, and bended at the initial region arising from the adsorption of oxidized species.[46] According to the slopes of the linear region of these curves, the electrochemically active surface areas of GF-1, GF-2 and GF-3 were calculated to be 0.107, 0.246, and 0.310 cm^2 respectively. Considering the active surface area of bare gold substrate was ≈0.034 cm^2, the roughness factors (R_f) of GF-1, GF-2 and GF-3 were estimated to be 3.1, 7.2 and 9.1. In addition, to assess the binding stability at the interface between the graphene films and gold substrate, the fabricated GFs were consecutively scanned for 50 cycles with CVs and the corresponding signal responses were recorded. As shown in Figure S4 (Supporting Information), only subtle

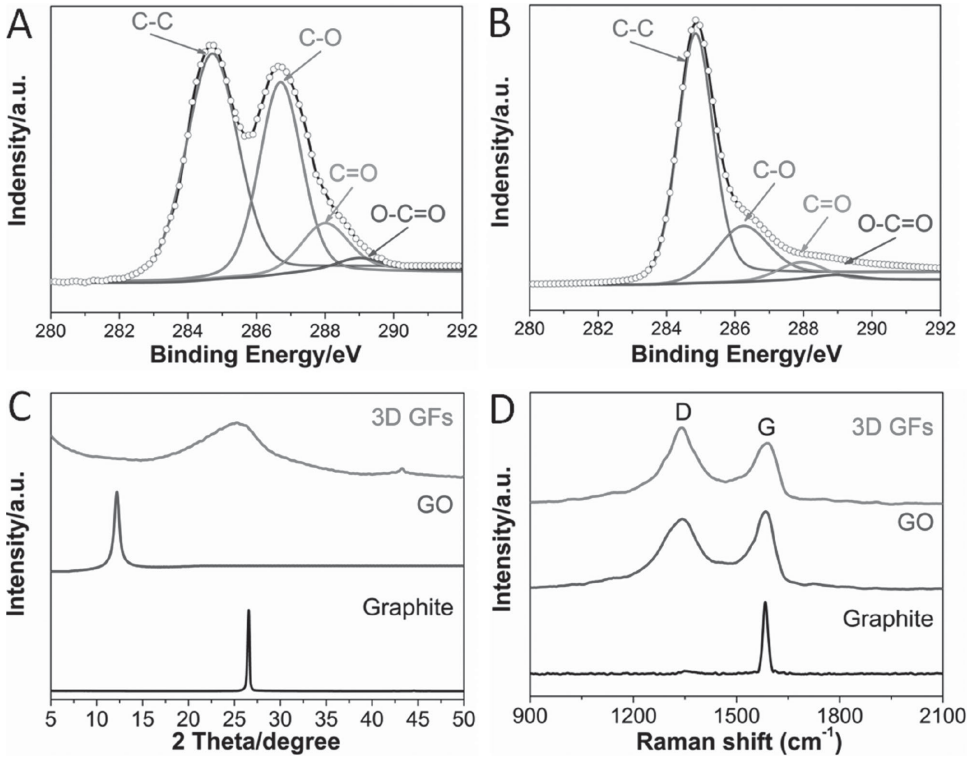

Figure 4. The C1s XPS spectra of A) GO, B) GFs. C) XRD patterns, D) Raman spectra of graphite, GO, and GFs.

current changes (ca. 4.5% in GF-1, 3.9% in GF-2 and 2.8% in GF-3) were observed in the CVs, demonstrating that an excellent binding strength was achieved in the proposed 3D GFs modified gold substrates. Meanwhile, EIS was adopted to investigate the interfacial electron transfer resistance (R_{et}) of different GFs. As shown in Figure 5B, compared with a large R_{et} of 14.6 Ω on bare gold substrate, smaller semicircles of 10.1 Ω, 6.2 Ω, and 5.3 Ω were obtained from GF-1 to GF-3 respectively, indicating that lower electron transfer resistance and high conductivity were produced on the porous graphene films.

All of these explorations confirmed that the proposed 3D GFs possessed controllable pore structures, significantly enhanced surface area, stable binding on the substrates, and high conductivity, all of which would make them promising candidates in the construction of novel electrochemical aptasensors with high performance.

2.3. Construction of the 3D GFs based Electrochemical Aptasensors for the Assay of ATP and Tob

ATP and Tob are two important molecules in composing and maintaining life activities. ATP plays an essential role in replication in all known living systems, and it is a critical component of many biological cofactors.[47] Tob is an extracellular serine protease and plays crucial roles in the blood coagulation cascade, thrombosis and haemostasis.[48] Meanwhile, it is known that ATP is a small linear biomolecule while Tob is a large one

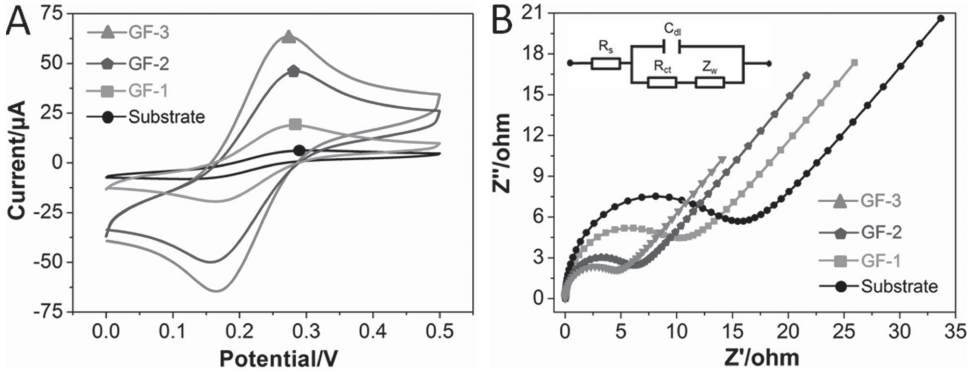

Figure 5. A) CVs and B) EIS characteriziaitons of the fabricated 3D GFs.

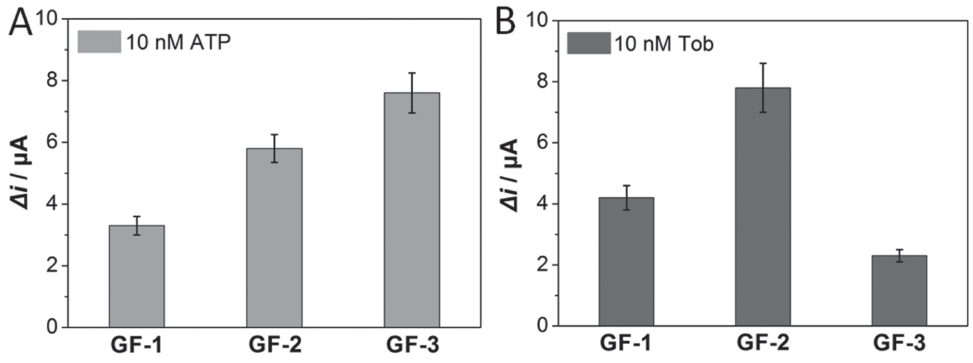

Figure 6. The signal changes in the presence of A) 10 nM ATP and B) 10 nM Tob based on various 3D GFs.

analogous with a cube with a diameter of 5 nm. Therefore, it is expectative to inspect the responses to the ATP and Tob based on 3D GFs with different structures and demonstrate the superior ability of the proposed GFs in the sensing applications.

Accordingly, electrochemical aptasensors were constructed for the assay of ATP and Tob respectively. The sensing scheme was designed on a facile strategy, which was shown in Figure 1B. The aptamer probes of ATP or Tob were firstly immobilized on the porous graphene surface through the strong π–π interaction between oligonucleotides and graphene.[49–51] In this condition, the electrochemical indicator of Ferrocene (Fc) at the terminal of aptamer probes was fixed approximately on the graphene surface and an intense signal response would be obtained. Once the target of ATP or Tob was added into the assay system, the aptamer would bind tightly and specifically to its target molecule to form a tertiary complex with more stable structure. Subsequently, the complex was disassociated from the graphene surface, resulting in an obvious decrease in the response signals.

2.4. Electrochemical Investigations of the Fabricated Aptasensors

As different interfacial micro-environments were observed with increased contact angles from GF-1 to GF-3, the effect of the immobilization time of aptamer probes on the signal responses was firstly investigated. SWV measurements were introduced to record the signals, which were found to provide excellent resolution of the electrochemical responses. As shown in Figure S5A (Supporting Information), due to increased surface area from the GF-1 to GF-3, more Apt-A was immobilized on the graphene surface and increased signal responses ranging from 9.0 μA, 11.5 μA to 13.9 μA were obtained respectively. As large contact angles made the linear aptamer sequences slightly difficult to transfer and interact with the graphene, more immobilization time was required to reach the current plateaus from GF-1 to GF-3 and ca. 9 h was needed in the case of GF-3. In addition, similar results were observed with Apt-T (Figure S5B, Supporting Information), on account of the analogous base sequences in the aptamers of ATP and Tob.

The feasibility of the proposed sensing scheme was also explored. ATP or Tob with a concentration of 10 nM were injected into the assay system, and the signal response changes (Δi, the changes of peak current before/after the addition of analyte) were monitored accordingly. As shown in **Figure 6**A, in the case of ATP, current changes of 3.3 μA (GF-1), 5.8 μA (GF-2), and 7.6 μA (GF-3) were obtained respectively. Meanwhile, the obvious current changes of 4.2 μA (GF-1), 7.8 μA (GF-2) and 2.3 μA (GF-3) were observed with Tob, as shown in Figure 6B. These results indicated that the sensing scheme was effective for the detection of ATP and Tob on 3D GFs. However, as a large current change was found on the GF-3 in the assay of ATP, a more sensitive signal response was acquired on the GF-2 in the assay of Tob, which may be attributed to the distinct interfacial micro-environments on the porous structures. In the assay of small ATP molecules, the ATP could sufficiently utilize porous structures and bind with Apt-A immobilized on the graphene surface, therefore an obvious signal change was observed in the GF-3 with a larger surface area. In the case of large Tob molecules, the diminished pore structure and increased contact angle on the GF-3 hindered them to effectively interact with the Apt-T on the surface, resulting in a small signal change. In contrary, improved interfacial environment was observed on the GF-2 with large pore structures, which facilitated the recognition between Tob and Apt-T and a larger signal response was obtained consequently. The results exhibited that the surface area, as well as interfacial micro-environments, played critical roles in the molecular recognitions.

2.5. Performance of the Fabricated Aptasensors

The sensitivities of the electrochemical aptasensors based on various 3D GFs were further investigated by varying the concentrations of the ATP or Tob, and the SWV was implemented to monitor the Δi. Based on the GF-3 and GF-2, the current signals for the detection of ATP (**Figure 7**A) and Tob (Figure 7C) decreased with the increment of ATP or Tob concentrations. As shown in Figure 7B and Figure 7D, the calibration plots showed a good linear relationship between the peak current changes and the concentrations of analytes. In the assay of ATP, a more sensitive regression equation of $\Delta i = 31.17 + 3.02 \text{Log}C_{\text{ATP}}$ ($R^2 = 0.992$) was obtained on the GF-3 (Figure 7B). While in the assay of Tob, a more sensitive regression equation of $\Delta i = 26.77 + 2.41 \text{Log}C_{\text{Tob}}$ ($R^2 = 0.997$) was observed

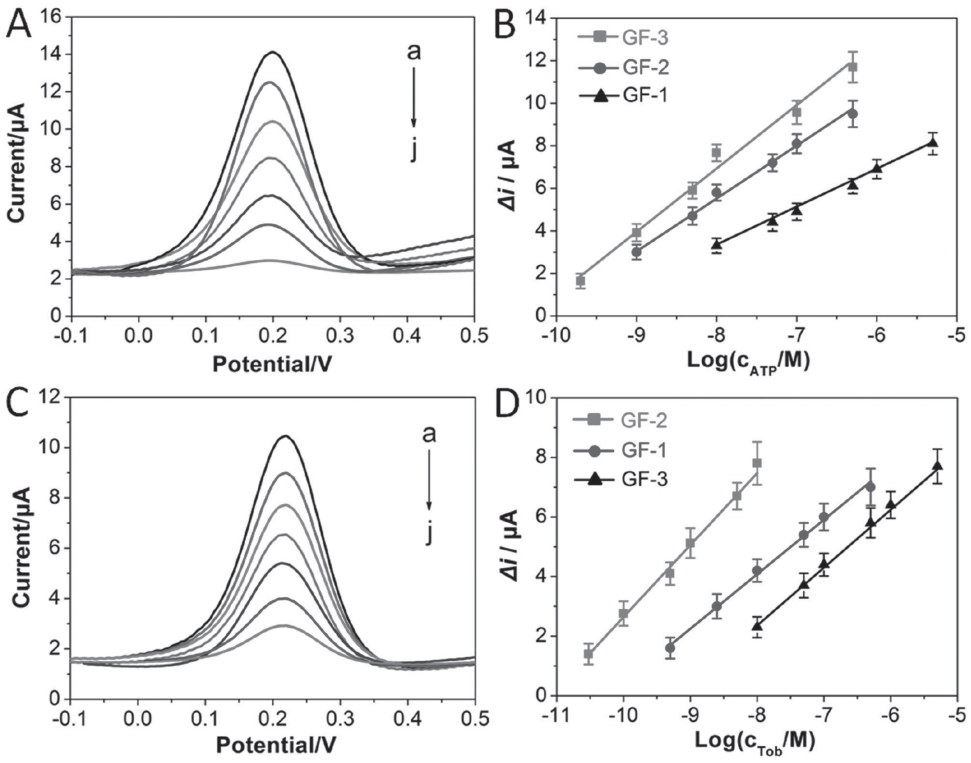

Figure 7. A) SWV responses of the ATP aptasensor based on GF-3 after incubation with ATP of different concentrations (a–j: 0 pM, 0.2 nM, 1 nM, 5 nM, 10 nM, 100 nM, and 500 nM). B) Calibration curves for the assay of ATP based on various 3D GFs. C) SWV responses of the Tob aptasensor based on GF-2 after incubation with Tob of different concentrations (a–j: 0 pM, 30 pM, 0.1 nM, 0.5 nM, 1 nM, 5 nM, and 10 nM). D) Calibration curves for the assay of Tob based on various 3D GFs.

on the GF-2 (Figure 7D). Based on the developed aptasensors, an impressive detection limit of 100 pM for ATP with a linear range from 0.2 nM to 500 nM was obtained on the GF-3, while a sensitive limit of 10 pM for Tob with a linear range from 30 pM to 10 nM was achieved on the GF-2 ($S/N = 3$). Considering the simple assay system without introducing any signal amplification steps, the detection limits of 100 pM in ATP and 10 pM in Tob were satisfactory, which were even comparable to those reported in some literatures (typically 0.2 nM to 100 nM for ATP and 30 pM to 6.4 nM for Tob),[52–60] shown in Table S1 (Supporting Information). As comparisons, ATP and Tob aptasensors based on the compact graphene film (C-GF) were also constructed here. The C-GF was treated with the natural drying, during which the residual water in the porous graphene film was dislodged through the capillary force, eventually leading to the agglomeration of the graphene sheets (Figure S6A, Supporting Information). Due to the significantly diminished surface area and increased electron transfer resistance of the C-GF (Figure S6B, Supporting Information), higher detection limits of 200 nM and 70 nM were observed in the detection of ATP and Tob respectively under the same conditions during the assay (Figure S6C,D, Supporting Information). It should be noted that the sensitivity of the porous GFs based aptasensors was tremendously higher than that based on the C-GF, confirming that the significantly enhanced surface area, as well as high electron transfer rate played a critical role in the ultrasensitive assay.

In addition to the sensitivity of an aptasensor, the specificity, stability and reproducibility were also extremely important for the practical applications. The specificity of the ATP aptasensor was determined by challenging it with 1 nM ATP, 1 mM CTP, 1 mM GTP, 1 mM UTP, and a mixture of them. While the specificity of the Tob aptasensor was checked by challenging it with 1 nM Tob, 1 mM Lzm, 1 mM BSA, 1 mM IgG and a mixture of them. As shown in **Figure 8**A,B, the proposed aptasensors showed an almost neglectable response to other interference analytes. The results indicated that the aptasensor possessed excellent selectivity in the assay of ATP or Tob, attributed to the highly specific interactions between the aptamers and related analytes.

Furthermore, the different aptamer probes immobilized graphene electrodes were firstly stored in the refrigerator at 4 °C for 1 week, 2 weeks and 3 weeks respectively, and then examined after adding the corresponding analytes. The results of the experiments showed that the ATP and Tob aptasensors retained about 82.0% and 82.3% of their initial responses respectively even after 3 weeks (Figure 8C), indicating the stability of the fabricated aptasensors was acceptable.

In order to inspect the reproducibility of the aptasensors, five freshly modified electrodes were incubated with 1 nM ATP or 1 nM Tob. All five electrodes exhibited a similar amperometric response, and the relative standard deviations (RSD) were 2.4% and 2.2% for ATP and Tob respectively (Figure 8D), demonstrating that the reproducibility of the proposed aptasensors was excellent.

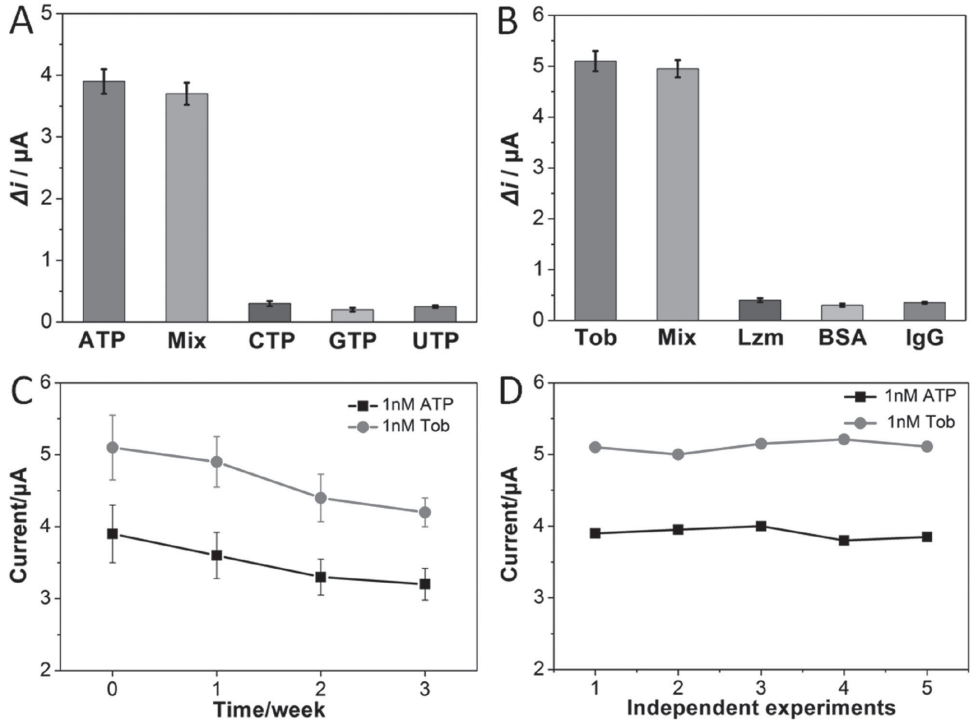

Figure 8. A) Selectivity evaluation of the ATP aptasensor based on GF-3 for 1 nM ATP against 1 mM CTP, 1 mM GTP, 1 mM UTP and a mixture respectively. B) Selectivity evaluation of the Tob aptasensor based on GF-2 for 1 nM Tob against 1 mM Lzm, 1 mM BSA, 1 mM IgG and a mixture respectively. C) Stability, and D) reproducibility tests of the ATP (based on GF-3) and Tob (based on GF-2) aptasensors.

Owing to the excellent sensitivity and selectivity of the proposed aptasensors, here we assessed the performance in the detection of the ATP and Tob in real human serum based on GF-3 and GF-2 respectively. The blank human serum was firstly diluted 100 times and detected according to the obtained calibration plots. Around 0.8 nM ATP (RSD = 3.8%) and no Tob were found in the blank serum sample. The standard addition method was then employed to evaluate the applicability of the aptasensors. The background signal arising from the serum sample was deducted in the quantitative assay. The analytical results for ATP and Tob were shown in **Table 1**. From the Table 1, we could see that the recovery (99.4% to 102% for ATP, 99.6% to 101% for Tob) and RSD (4.1% to 5.0% for ATP, 3.8% to 4.9% for Tob) were satisfactory, which clearly suggested the aptasensors possessed a promising potential for the detection of ATP and Tob in real biological samples.

Table 1. Assay results of ATP and Tob in human serum sample.

Samples	Added	Founded	Recovery [%]	RSD [%]
ATP	100 pM	99.5 pM	99.5	5.0
ATP	1.00 nM	1.02 nM	102	4.5
ATP	5.00 nM	4.97 nM	99.4	4.1
Tob	100 pM	99.7 pM	99.7	4.9
Tob	1.00 nM	1.01 nM	101	4.2
Tob	5.00 nM	4.98 nM	99.6	3.8

3. Conclusion

In summary, for the first time, we demonstrated a facile and reliable approach for in situ fabrication of 3D GFs with controllable pore structures on gold substrates. The produced GFs possessed some prominent properties, for example, significantly enlarged surface area, excellent binding strength on the substrates and high conductivity, which would enable many advanced applications. As selected examples, GFs based electrochemical aptasensors in the assay of ATP and Tob, exhibited high sensitivity, and excellent selectivity, stability and reproducibility, as well as promising potential in real serum sample analysis. It is believed that the proposed approach can provide a new reference for in situ fabrication of more graphene films and the as-synthesized 3D GFs would open up a wide horizon for promising applications in electronic and energy-related systems.

4. Experimental Section

Materials and Agents: Natural graphite powder (325 meshes) was obtained from Qingdao Huatai Lubricant Sealing S&T Co. Ltd., China. 4-Aminothiophenol, tris(hydroxymethyl)aminomethane (Tris-base), 1-ethyl-(3–3′-dimethylaminopropyl) carbodiimide (EDC), Nhydroxysuccinimide (NHS), thrombin (Tob), lysozyme (Lzm), bovine serum albumin (BSA), hemoglobin (Hb), adenosine triphosphate (ATP), cytidine triphosphate (CTP), uridine triphosphate (UTP) and guanosine triphosphate (GTP) were obtained from Sigma-Aldrich. Silica spheres (0.5 and 0.25 μm, 10 wt%) were purchased from Polysciences Inc. Sulfuric acid, potassium permanganate, hydrogen peroxide and

hydrochloric acid were got from Sinopharm Chemical Reagent Co., Ltd. All oligonucleotides were synthesized by TaKaRa biotechnology Co., Ltd. (Dalian, China). Aptamer for ATP (Apt-A): 5′-GCA CCT GGG GGA GTA TTG CGG AGG AAG GT-Ferrocene (Fc)-3', Aptamer for Tob (Apt-T): 5′-AGT CCG TGG TAG GGC AGG TTG GGG TGA CT-Fc-3′. Other chemicals employed were all of analytical grade and triple distilled water was used throughout.

Synthesis of Graphene Oxide (GO): GO was prepared by the oxidation of natural graphite powder according to a modified Hummers' method, as reported elsewhere.[61] In brief, graphite was added to concentrated sulfuric acid under stirring, and then sodium nitrate was added. Under vigorous agitation, potassium permanganate was added slowly at a temperature of 10 °C. Successively, the reaction system was transferred to a water bath for about 1 h, forming a thick paste. Then, additional water was added, and the solution was stirred for another 30 min. Subsequently, hydrogen peroxide was slowly added, turning the color of the solution from brown to yellow. The mixture was filtered and washed with hydrochloric acid aqueous solution to remove metal ions, followed by thoroughly washing with water and centrifuging to remove the acid. The resulting solid was dispersed in water by ultrasonication, and it was purified by dialysis to remove the remaining salt impurities.

In Situ Fabrication of 3D GFs on Gold Substrates: The gold substrate was firstly pretreated following a known procedure.[62] The freshly cleaned substrate was immersed into a 4-aminothiophenol ethanol solution (0.5 mM) for 1 h to form the SAM, which was subsequently rinsed with ethanol. The precursor solution containing GO (2 mg/mL, 2 mL) and SiO_2 spheres (10 μL) was sufficiently mixed with the ultrasonication for 15 min. The modified gold substrate was placed vertically into the precursor solution and left at room temperature for 6 h, followed by heating in a Teflon-lined autoclave at 160 °C for 6 h. Coupling agents of EDC and NHS were introduced to promote the condensation reaction between the $–NH_2$ groups at the terminal of SAM and –COOH groups of the GO to form a covalent amide bond (CO–NH).[63,64] After the HR treatment, the gold substrate was dipped into the HF solution to remove silica spheres and sufficiently washed with distilled water, and then treated with a freeze drying. The porous graphene films fabricated without silica spheres and with the silica spheres of 500 nm and 250 nm were denominated as GF-1, GF-2, and GF-3 respectively. Besides, as a comparison, a compact graphene film (C-GF) was prepared with a similar procedure used in the fabrication of GF-1, in which a natural drying instead of freeze drying was introduced.

Material Characterizations: The morphologies of the 3D GFs were observed by field-emission scanning electron microscopy (FESEM, Hitachi S4800). Analysis of the X-ray photoelectron spectra (XPS) was performed on an ESCLAB MKII. X-ray diffraction (XRD) was measured on an X-ray diffractometer (D/MAX 2500 V/PC) with a Cu-Ka line (0.15419 nm). Raman measurements were conducted on a LabRam-1B Raman spectroscope equipped with a 514 nm laser source. Contact angles were measured on a drop shape analysis system G10/DSA10 contact angle system, and a water droplet (5 μL) was dropped on the surface of 3D GFs.

Construction of the 3D GFs Based Aptasensors for Assay of ATP and Tob: The 3D GFs modified gold substrates were immersed into an immobilization buffer of Tris-HCl (10 mM), EDTA (1 mM) and NaCl (0.1 M) at pH 7.4 containing aptamer probes (2 μM) of ATP or Tob for a definite time, and the unbound probes were sufficiently washed away with washing buffer (10 mM Tris-HCl, pH 7.4). Subsequently, the sensing interfaces were treated with the solution containing the ATP or Tob with various concentrations, again followed by thoroughly washing with the Tris-HCl (10 mM).

Electrochemical Measurements: All electrochemical measurements were performed with a CHI 660C electrochemical workstation (Shanghai Chenhua, China). The three-electrode system used consisting of 3D GFs modified working electrode, a platinum auxiliary electrode, and an Ag/AgCl (saturated KCl) reference electrode. Cyclic voltammetry (CV) was carried out at a scan rate of 100 mV/s, square wave voltammetric (SWV) measurements were taken at a frequency of 5 Hz, and electrochemical impedance spectroscopy (EIS) measurements were performed with the frequency changed from 0.01 Hz to 100 kHz with signal amplitude of 5 mV. The chronocoulometric (CC) curve was introduced to measure the active surface area of proposed 3D GFs. During the CC measurement, $K_3Fe(CN)_6$ aqueous solution (1 mM) containing KCl (2 M) was served as the electrochemical indicator and a nitrogen atmosphere was maintained to avoid air sliding into the electrochemical cell.

Quantitative Assay of ATP and Tob in Human Serum: Healthy human serum was used to confirm the applicability of fabricated aptasensors. The serum sample was loaded into a centrifugal filter device, and subjected to centrifugation (12 000*g*, 15 min). The serum centrifugation ultrafiltrate was diluted 100 times and used for the following measurements. The concentrations of ATP and Tob in the blank serum sample were firstly detected by the obtained calibration plots of aptasensors, and the background signals would be deducted in the subsequent quantitative assay. Then standard solutions of ATP or Tob with different concentrations were added into the diluted serum and the electrochemical assays were performed.

Supporting Information

Supporting Information is available from the Wiley Online Library or from the author.

Acknowledgements

This work was supported by the Innovative Research Team Program by the Ministry of Education of China (No. IRT13070), the Doctoral Fund of Ministry of Education of China (No. 20113221110001) and A Project Funded the Priority Academic Program Development of Jiangsu Higher Education Institutions (PAPD). Figures 1 and 3 were revised on November 26, 2014.

Received: June 24, 2014
Revised: August 11, 2014
Published online: September 5, 2014

[1] A. K. Geim, *Science* **2009**, *324*, 1530.
[2] A. K. Geim, K. S. Novoselov, *Nat. Mater.* **2007**, *6*, 183.
[3] C. Li, G. Shi, *Nanoscale* **2012**, *4*, 5549.
[4] S. Yin, Z. Niu, X. Chen, *Small* **2012**, *8*, 2458.
[5] S. Chen, S. Z. Qiao, *ACS Nano* **2013**, *7*, 10190.
[6] F. He, N. Niu, F. Qu, S. Wei, Y. Chen, S. Gai, P. Gao, Y. Wang, P. Yang, *Nanoscale* **2013**, *5*, 8507.
[7] Y. Zhao, J. Liu, Y. Hu, H. Cheng, C. Hu, C. Jiang, L. Jiang, A. Cao, L. Qu, *Adv. Mater.* **2013**, *25*, 591.
[8] Y. Yang, X. Fan, G. Casillas, Z. Peng, G. Ruan, G. Wang, M. J. Yacaman, J. M. Tour, *ACS Nano* **2014**, *8*, 3939.
[9] X. Dong, X. Wang, L. Wang, H. Song, H. Zhang, W. Huang, P. Chen, *ACS Appl. Mater. Inter.* **2012**, *4*, 3129.
[10] V. Penmatsa, T. Kim, M. Beidaghi, H. Kawarada, L. Gu, Z. Wang, C. Wang, *Nanoscale* **2012**, *4*, 3673.
[11] H. Sun, Z. Xu, C. Gao, *Adv. Mater.* **2013**, *25*, 2554.
[12] L. Qiu, J. Z. Liu, S. L. Y. Chang, Y. Wu, D. Li, *Nat. Commun.* **2012**, *3*, 1241.
[13] Z. S. Wu, Y. Sun, Y. Z. Tan, S. Yang, X. Feng, K. Muellen, *J. Am. Chem. Soc.* **2012**, *134*, 19532.
[14] Y. Zhao, J. Liu, Y. Hu, H. Cheng, C. Hu, C. Jiang, L. Jiang, A. Cao, L. Qu, *Adv. Mater.* **2013**, *25*, 591.
[15] Y. Xu, K. Sheng, C. Li, G. Shi, *ACS Nano* **2010**, *4*, 4324.
[16] K. Sheng, Y. Sun, C. Li, W. Yuan, G. Shi, *Sci. Rep.* **2012**, *2*, 247.
[17] K. Chen, L. Chen, Y. Chen, H. Bai, L. Li, *J. Mater. Chem.* **2012**, *22*, 20968.

[18] M. Hilder, B. Winther-Jensen, D. Li, M. Forsyth, D. R. MacFarlane, *Phys. Chem. Chem. Phys.* **2011**, *13*, 9187.
[19] Z. Chen, W. Ren, L. Gao, B. Liu, S. Pei, H. M. Cheng, *Nat. Mater.* **2011**, *10*, 424.
[20] J. C. Yoon, J. S. Lee, S. I. Kim, K. H. Kim, J. H. Jang, *Sci. Rep.* **2013**, *3*, 1788.
[21] Z. L. Wang, D. Xu, H. G. Wang, Z. Wu, X. B. Zhang, *ACS Nano* **2013**, *7*, 2422.
[22] S. Yin, Y. Zhang, J. Kong, C. Zou, C. M. Li, X. Lu, J. Ma, F. Y. C. Boey, X. Chen, *ACS Nano* **2011**, *5*, 3831.
[23] Y. Han, Z. Xu, C. Gao, *Adv. Funct. Mater.* **2013**, *23*, 3693.
[24] W. Yuan, A. Liu, L. Huang, C. Li, G. Shi, *Adv. Mater.* **2013**, *25*, 766.
[25] A. A. Lubin, K. W. Plaxco, *Acc. Chem. Res.* **2010**, *43*, 496.
[26] I. Willner, M. Zayats, *Angew. Chem. Int. Ed.* **2007**, *46*, 6408.
[27] W. Tan, M. J. Donovan, J. Jiang, *Chem. Rev.* **2013**, *113*, 2842.
[28] L. Shi, Z. Chu, Y. Liu, W. Jin, X. Chen, *Biosens. Bioelectron.* **2014**, *54*, 165.
[29] W. Zhang, K. Patel, A. Schexnider, S. Banu, A. D. Radadia, *ACS Nano* **2014**, *8*, 1419.
[30] E. Vasilyeva, B. Lam, Z. Fang, M. D. Minden, E. H. Sargent, S. O. Kelley, *Angew. Chem. Int. Ed.* **2011**, *50*, 4137.
[31] L. P. Xu, S. Wang, H. Dong, G. Liu, Y. Wen, S. Wang, X. Zhang, *Nanoscale* **2012**, *4*, 3786.
[32] L. Shi, Z. Chu, Y. Liu, J. Peng, W. Jin, *J. Mater. Chem. B* **2014**, *2*, 2658.
[33] M. Kind, C. Woell, *Prog. Surf. Sci.* **2009**, *84*, 230.
[34] C. Vericat, M. E. Vela, G. Benitez, P. Carro, R. C. Salvarezza, *Chem. Soc. Rev.* **2010**, *39*, 1805.
[35] L. Shi, Z. Chu, X. Dong, W. Jin, E. Dempsey, *Nanoscale* **2013**, *5*, 10219.
[36] H. Yabu, M. Takebayashi, M. Tanaka, M. Shimomura, *Langmuir* **2005**, *21*, 3235.
[37] M. T. Khorasani, H. Mirzadeh, Z. Kermani, *Appl. Surf. Sci.* **2005**, *242*, 339.
[38] L. Shi, Z. Chu, Y. Liu, W. Jin, X. Chen, *Biosens. Bioelectron.* **2013**, *49*, 184.
[39] M. Jin, T. H. Kim, S. C. Lim, D. L. Duong, H. J. Shin, Y. W. Jo, H. K. Jeong, J. Chang, S. Xie, Y. H. Lee, *Adv. Funct. Mater.* **2011**, *21*, 3496.
[40] J. Chen, K. Sheng, P. Luo, C. Li, G. Shi, *Adv. Mater.* **2012**, *24*, 4569.
[41] H. S. Ahn, J. W. Jang, M. Seol, J. M. Kim, D. J. Yun, C. Park, H. Kim, D. H. Youn, J. Y. Kim, G. Park, S. C. Park, J. M. Kim, D. I. Yu, K. Yong, M. H. Kim, J. S. Lee, *Sci. Rep.* **2013**, *3*, 1396.
[42] S. H. Lee, H. W. Kim, J. O. Hwang, W. J. Lee, J. Kwon, C. W. Bielawski, R. S. Ruoff, S. O. Kim, *Angew. Chem. Int. Ed.* **2010**, *49*, 10084.
[43] A. C. Ferrari, J. C. Meyer, V. Scardaci, C. Casiraghi, M. Lazzeri, F. Mauri, S. Piscanec, D. Jiang, K. S. Novoselov, S. Roth, A. K. Geim, *Phys. Rev. Lett.* **2006**, *97*, 187401.
[44] L. Shi, Z. Chu, Y. Liu, W. Jin, X. Chen, *Biosens. Bioelectron.* **2013**, *49*, 184.
[45] X. Yu, K. Sheng, G. Shi, *Analyst* **2014**,139, 4525.
[46] M. Zhou, Y. Zhai, S. Dong, *Anal. Chem.* **2009**, *81*, 5603.
[47] M. M. Gottesman, T. Fojo, S. E. Bates, *Nat. Rev. Cancer* **2002**, *2*, 48.
[48] C. T. Esmon, *Thromb. Haemost.* **2014**, *111*, 625.
[49] A. Bonanni, M. Pumera, *ACS Nano* **2011**, *5*, 2356.
[50] L. Wang, M. Xu, L. Han, M. Zhou, C. Zhu, S. Dong, *Anal. Chem.* **2012**, *84*, 7301.
[51] Y. Tao, Y. Lin, J. Ren, X. Qu, *Biomaterials* **2013**, *34*, 4810.
[52] L. Hu, Z. Bian, H. Li, S. Han, Y. Yuan, L. Gao, G. Xu, *Anal. Chem.* **2009**, *81*, 9807.
[53] N. Liu, Y. Jiang, Y. Zhou, F. Xia, W. Guo, L. Jiang, *Angew. Chem. Int. Ed.* **2013**, *52*, 2007.
[54] H. Zhang, Y. Han, Y. Guo, C. Dong, *J. Mater. Chem.* **2012**, *22*, 23900.
[55] X. Zuo, S. Song, J. Zhang, D. Pan, L. Wang, C. Fan, *J. Am. Chem. Soc.* **2007**, *129*, 1042.
[56] N. N. Bu, A. Gao, X. W. He, X. B. Yin, *Biosens. Bioelectron.* **2013**, *43*, 200.
[57] X. X. Jiao, J. R. Chen, X. Y. Zhang, H. Q. Luo, N. B. Li, *Anal. Biochem.* **2013**, *441*, 95.
[58] Y. Xiao, A. A. Lubin, A. J. Heeger, K. W. Plaxco, *Angew. Chem. Int. Ed.* **2005**, *44*, 5456.
[59] Y. Xiao, B. D. Piorek, K. W. Plaxco, A. J. Heeger, *J. Am. Chem. Soc.* **2005**, *127*, 17990.
[60] M. Mir, M. Vreeke, L. Katakis, *Electrochem. Commun.* **2006**, *8*, 505.
[61] Y. Xu, L. Zhao, H. Bai, W. Hong, C. Li, G. Shi, *J. Am. Chem. Soc.* **2009**, *131*, 13490.
[62] J. Zhang, S. Song, L. Wang, D. Pan, C. Fan, *Nat. Protoc.* **2007**, *2*, 2888.
[63] M. Mikhaylova, D. K. Kim, C. C. Berry, A. Zagorodni, M. Toprak, A. S. G. Curtis, M. Muhammed, *Chem. Mater.* **2004**, *16*, 2344.
[64] K. Susumu, H. T. Uyeda, I. L. Medintz, T. Pons, J. B. Delehanty, H. Mattoussi, *J. Am. Chem. Soc.* **2007**, *129*, 13987.